Available online at www.sciencedirect.com
SCIENCE DIRECT
Journal of Solid State Chemistry 179 (2006) 1782–1791
JOURNAL OF SOLID STATE CHEMISTRY
www.elsevier.com/locate/jssc

A high-temperature structure for Ta_2O_5 with modulations by TiO_2 substitution

Darko Makovec[a,b,*], Jian-Min Zuo[b,c], Ray Twesten[b], David A. Payne[b,c]

[a]*Jožef Stefan Institute, Jamova 39, Si-1000 Ljubljana, Slovenia*
[b]*Frederick Seitz Materials Research Laboratory, University of Illinois at Urbana-Champaign, USA*
[c]*Department of Materials Science and Engineering, University of Illinois at Urbana-Champaign, USA*

Received 19 October 2005; received in revised form 14 February 2006; accepted 16 March 2006
Available online 22 March 2006

Abstract

Solid solutions in the series $(1-x)Ta_2O_5-xTiO_2$ with $x = 0.0-0.1$ were prepared by high-temperature ceramic processing methods, and the crystal structure was determined at room temperature by transmission electron microscopy, electron diffraction and high-resolution lattice imaging. A structural model is proposed for the oxygen-deficient tantalum oxide (Ta_2O_5) phase with high TiO_2 doping level ($x = 0.08$). The model is based on edge sharing of an oxygen octahedron–hexagonal bi-pyramid–octahedron molecular building block unit that repeats *four* times per unit cell. Electron diffraction reveals a monoclinic distortion from a pseudo-tetragonal model structure that is modulated primarily along $\langle 110 \rangle$. The modulation length varies with increasing TiO_2 content. Furthermore, by quantitative HREM analysis and matching of lattice images by simulation, it is shown that the modulation is associated with small ionic displacements in specific lattice planes that coincide with Ta ions in the model structure coordinated by oxygen hexagonal bi-pyramids. Based on this evidence, it is suggested that the modulation comes from a replacement of Ta with Ti ions, and the loss of inversion symmetry in the modulated structure is related to the dielectric properties of the material.

Keywords: Tantalum oxide; Structure; Structural modulations; Dielectric properties; Electron microscopy; High-resolution imaging; Electron diffraction

1. Introduction

Tantalum oxide (Ta_2O_5) is a useful material that enables a variety of technological applications, ranging from electrolytic capacitors to thermal-barrier coatings. Several crystal structures have been reported that depend on the particular thermal-processing conditions used, and additives chosen. In this paper, we report the room-temperature structure for compositions in the $(1-x)Ta_2O_5$–$xTiO_2$ system ($x<0.1$) after heat treatment at 1400 °C. Electron microscopy was used to determine the structure.

Ta_2O_5 is a refractory oxide (m. pt. = 1872 °C), stable in air, and chemically inert. A sluggish and reversible phase transformation occurs at ~1360 °C for pure Ta_2O_5 [1], but the nature of the structure for each phase is still uncertain [2]. The lower-temperature phase (L-Ta_2O_5) appears to be orthorhombic [3–8], though a smaller-unit-cell hexagonal structure has been reported [9–11]. The high-temperature phase (H-Ta_2O_5) appears to be tetragonal, but various metastable phases can form on cooling. At room temperature, "H-Ta_2O_5" in meta-stable form exhibits monoclinic (or triclinic) symmetry that is slightly distorted from tetragonal [3,12–15].

Additions of TiO_2 lower the temperature of the L ⇒ H-Ta_2O_5 phase transformation, with a minimum transformation temperature of ~1150 °C for $(1-x)Ta_2O_5$–$xTiO_2$ at $\sim x = 0.09$. The solid-solubility limit is $x = 0.125$ for H-Ta_2O_5, and the reversion from the H- to L-structures is impeded with increasing TiO_2 content. The high-temperature structure is stabilized into different phases depending on TiO_2 concentrations. A sequence of phase transformations occurs on cooling [3,13,15].

As mentioned above, one application for Ta_2O_5 is in electrolytic capacitors. Anodized layers are typically

*Corresponding author. Jožef Stefan Institute, Jamova 39, Si-1000 Ljubljana, Slovenia. Fax: +386 1 4773 875.
E-mail address: darko.makovec@ijs.si (D. Makovec).

0022-4596/$ - see front matter © 2006 Elsevier Inc. All rights reserved.
doi:10.1016/j.jssc.2006.03.014

formed on Ta metal, and the oxide has a dielectric constant (K) of ≈ 25 in the amorphous state. Crystallization into the L-Ta_2O_5 structure (i.e., orthorhombic) increases the K value to ≈ 35. Cava et al. [16] reported an increase in K for $(1-x)Ta_2O_5$–$xTiO_2$ ceramics when fired in air at 1400 °C. A maximum value of $K = 126$ was given at $x = 0.08$. The increase in K was associated with the appearance of a monoclinic structure at room temperature. We have confirmed these findings and obtained higher values ($K = 340$ at $x = 0.056$ [17], and $K = 280$ at $x = 0.08$ [18]), presumably due to the preparation of more dense ceramic microstructures. Our higher-K values are associated with heat treatment above the phase-transformation temperature, and stabilization of a solid-solution H-Ta_2O_5 monoclinic structure at room temperature.

In this paper, we propose a new structural model for H-Ta_2O_5 stabilized at room temperature, and the effects of TiO_2 additions on structure are reported. Emphasis is paid to modulations in the monoclinic structure, and comparisons are made with an earlier model reported by Stephenson and Roth [16]. The results are of interest when capacitance densities greater than those obtained for pure Ta_2O_5 are required, and are significantly greater than SiO_2 currently used in the microelectronics industry. Future applications may include gate-oxide dielectrics for the miniaturization of integrated circuitry, if the H-Ta_2O_5 structure could be stabilized at lower temperatures.

2. Experimental

Ceramic specimens were prepared by mixed-oxide processing in the $(1-x)Ta_2O_5$–$xTiO_2$ system, for $x = 0$, 0.03, 0.056, 0.08 and 0.10. The starting materials were Ta_2O_5 (99.99% pure, L-Ta_2O_5, Cerac, Milwaukee, WI) and TiO_2 (99.9+ % pure, anatase, Aldrich, Milwaukee, WI). 100 g batches were mixed in suspension in Teflon containers using isopropanol and zirconia media. After drying the mixed powders were placed in covered Al_2O_3 crucibles, and reacted in an electrically heated furnace at 1000 °C for 5 h. The mixing and firing was repeated a second time to ensure the calcined powder was size reduced and homogeneously reacted. X-ray diffraction (XRD, Rigaku D-Max III) confirmed the formation of single-phase L-Ta_2O_5. The calcined product was size reduced again, dried and granulated into powder, and pressed into 1 cm diameter pellets, ~1.5 mm thick. The pressed pellets were then cold-isostatically pressed to densities approximating 55% of theoretical, before firing at 1400 °C for 16 h. A double-inverted Al_2O_3 crucible arrangement was used, and the specimens were covered with a powder of their own composition. The heating rate was 5 °C/min, and the cooling rate was initially 30 °C/min to 900 °C, followed by 10 °C/min to 400 °C. After firing, the ceramics were examined by microscopy and XRD. No L-Ta_2O_5 was detected. Thinned specimens were prepared for electron microscopy by grinding to $\approx 100\,\mu m$, core drilling 3 mm diameter discs, dimpling to 20 μm, and perforating by ion-beam milling (Ar, 5 kV, 12° incidence, 80 K). Microstructures were examined by transmission electron microscopy (TEM), and structural modulations were followed by electron diffraction. Direct imaging of the lattice structure was obtained through the use of a high-resolution pole piece ($c_s = 1.0$ mm, $c_c = 1.4$ mm), and the microscope was operated at 200 kV with a field-emission source (JEOL 2010 F TEM/STEM). For improved high-resolution imaging, it was found necessary to anneal the thinned specimens in air at 600 °C before examination. No L-Ta_2O_5 was detected by XRD in specimens prepared for TEM analysis.

In general, the electron diffraction patterns obtained for $(1-x)Ta_2O_5$–$xTiO_2$ were comprised of strong Bragg reflections, with weak reflections that could be attributed to structural modulations. The strong reflections can be indexed on the basic structure for H-Ta_2O_5. This is discussed below in Section 3.1 for $x = 0.08$. After establishing a pseudo-tetragonal model the effect of TiO_2 additions ($x = 0.03-0.1$) on weak reflections and deviations from tetragonality are considered in Section 3.2. The ionic displacements that give rise to the modulated distortions are associated with the enhancement in K observed for monoclinic "H-Ta_2O_5" at room temperature.

3. Results and discussion

3.1. Basic structure for H-Ta_2O_5

Fig. 1 shows electron diffraction patterns obtained for the $(1-x)Ta_2O_5$–$xTiO_2$ specimen $x = 0.08$, now referred to as $92Ta_2O_5$–$8TiO_2$, taken along four zone axes ([100], [001], [$\bar{1}$ $\bar{1}$ 0], and [$\bar{1}$ 1 0]). Apart from the strong reflections, weak reflections (i.e., resulting from structural modulations) were also visible along [001] and [$\bar{1}$ 1 0] zone axes. We indexed the strong reflections on a monoclinic cell with $a = 0.379$ nm, $b = 0.381$ nm, $c = 3.57$ nm, and $\beta = 90.8°$. The structure was previously determined by XRD and designated "$30{:}1_{SS}$" by Waring and Roth [3] or H1 monoclinic structure by Von Plies and Gruehn [15] Note, in our determination, the *pseudo-tetragonal* long axis is along c.

Now we present our electron diffraction and high-resolution imaging data for the basic unit cell, and later consider weak reflections and modulated structures.

3.1.1. Electron diffraction

For electron diffraction along the [100] zone axis (Fig. 1(a)), strong reflections occur at (0, 0, 2n) (n integer) positions along the c^* direction, at (0, 2n, 0) along the b^* direction, and at (0, 1, 2n+1). The diffraction pattern along [010] direction has the same characteristics as along [100] for the strong reflections, but with a small distortion. For electron diffraction along the [001] zone axis (Fig. 1(b)), reflections at (h, 0, 0) and (0, k, 0) positions are stronger for h, $k = 2n$ than h, $k = 2n + 1$ (n integer). Along the [$\bar{1}$ $\bar{1}$ 0] zone axis (Fig. 1(c)) strong reflections are

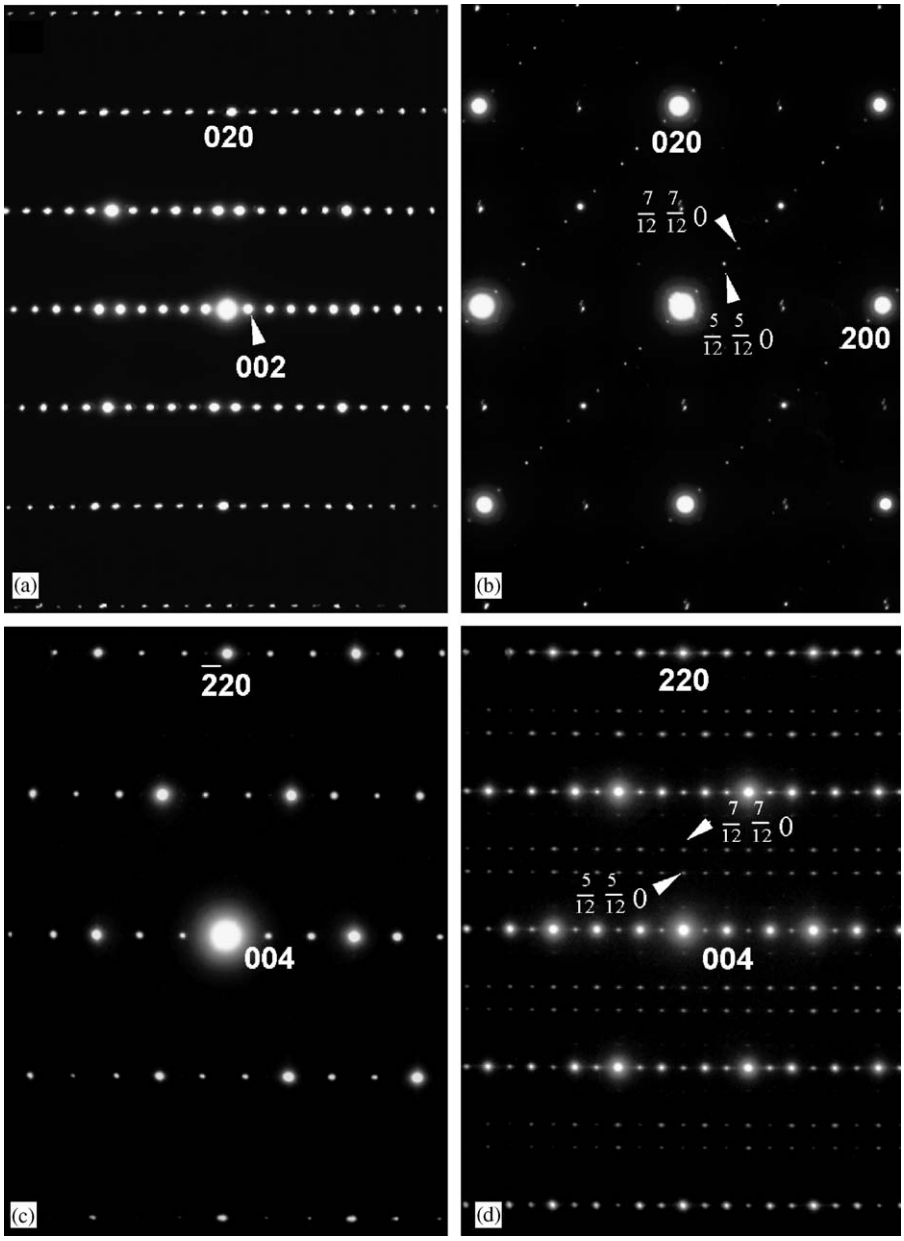

Fig. 1. Electron diffraction patterns for $92Ta_2O_5$–$8TiO_2$ along [100] zone axis (a), along [001] zone axis (b), along [$\bar{1}$ $\bar{1}$ 0] zone axis (c), and along [$\bar{1}$ 1 0] zone axis (d).

at (0, 0, 4*n*), (−2*n*, 2*m*, 0), and (−1, 1, 2*n*) positions, while diffra-
ction spots at (0, 0, 2*n*) and (−2*n*+1, 2*m*+1, 0) (*n*, *m* integer) are noticeably absent. The electron diffraction pattern along the [$\bar{1}$ 1 0] zone axis (Fig. 1(d)) has the same characteristics as that along [$\bar{1}$ $\bar{1}$ 0] apart from the weak reflections from the structural modulations. The difference between monoclinic *a* and *b* axes is small and difficult to distinguish by electron diffraction. For this reason, we use *pseudo-tetragonal* indices to index experimental diffraction patterns.

The crystal structure of H-Ta_2O_5, originally proposed by Stephenson and Roth [14] from XRD analysis of 2 mol% Sc_2O_3-stabilized Ta_2O_5 single crystals, was reported to be monoclinic, face-centered space group *C*2, with $a = 3.5966$ nm, $b = 0.381$ nm, $c = 0.381$ nm, and $\beta = 96.12^\circ$. The unit cell was comprised of six Ta_2O_5 formula units. Note, the long axis was along *a*. Their structure can be considered in terms of tantalum cations surrounded by pentagonal bipyramids of oxygen anions (coordination 7) and distorted TaO_6^{7-} octahedra (coordination 6). This structure of H-Ta_2O_5 can be viewed as a modification of an idealized structure with intermix units of octahedra and hexagonal bipyramids. In this model the octahedra are either corner or edge shared. The ratio between octahedra and hexagonal bipyramid building blocks is 2:1. A local reduction in oxygen content is accommodated by crystallographic shear. In the case of Sc_2O_3-stabilized Ta_2O_5, it was suggested that

substitution of Sc^{3+} for Ta^{5+} caused a reduction in oxygen content that could be accounted for by random shear and transformation of hexagonal bi-pyramids.

For a face-centered monoclinic structure, the electron diffraction patterns should exhibit the extinction condition $h+k=2n$ for the C lattice. The long cell axis is taken as the a-axis in terms of the structure reported by Stephenson and Roth. Thus, in our pseudo-tetragonal index ($a \approx b$ and $c \gg a$), extinction occurs at $h+l=2n+1$ or $k+l=2n+1$. While the missing of (110) and (0, 0, $2l+1$) reflections in the [$\bar{1}$ 1 0] zone axis, and (1 $\bar{1}$ 0), (0, 0, $2l+1$) and (1, -1, $4n$) reflections in the [$\bar{1}$ $\bar{1}$ 0] zone axis, is consistent with the face-centered lattice, additional extinctions are also seen in our diffraction data. For example, reflections for (-1, 1, $2l+1$) and (0, 0, $4n+2$) are clearly absent in the [$\bar{1}$ $\bar{1}$ 0] zone axis diffraction pattern. Both (-1, 1, $2l+1$) and (0, 0, $4n+2$) are permitted by the consideration of the face-centered extinction rule. Along [001], the reflections of (110), ($\bar{1}$ 1 0), (100) and (010) are very weak (Fig. 1b). The fact that (100) and (110) are extinct in the other zone axes suggests that they come from a deviation in the ideal tetragonal structure. The deviation comes from structural modulations, which we explain later in Section 3.2.

There is also additional discrepancy between the structure of H-Ta_2O_5 reported by Stephenson and Roth and our high-resolution electron microscopy (HREM) results. Fig. 2 gives a HREM image along [$\bar{1}$ 1 0] taken near the Scherzer focus (≈ -50 nm). The basic pattern of the HREM image consists of a zig-zag chain of bright dots. To further clarify the HREM image, additional information was sought by atomic number (Z) contrast imaging in the high-angle annular dark-field mode (HAADF). This method gives compositional information for heavy ions, tantalum in this case, since it detects electrons scattered at high angles, where the intensity is dependent on Z, and Ta atoms dominate the image contrast, and appear bright. In comparison, the contrast of HREM images depends on both thickness and defocus. Fig. 3 shows one of the HAADF images obtained. The image has a stripe-like contrast, with each stripe consisting of three columns of bright dots, presumably for Ta ions. Examination of the patterning along the [110] projection (Fig. 3) gives a zig-zag arrangement for Ta ions, according to …$^{o\ o\ o}_{\ o\ o\ o}$…., which is consistent with the contrast in HREM (Fig. 2). In the structure according to Stephenson and Roth, Ta ions are arranged in the pattern of …$^{oo\ oo\ oo}_{\ o\ \ o\ \ o}$… when viewed along [110], which is different from that shown in our experimental images.

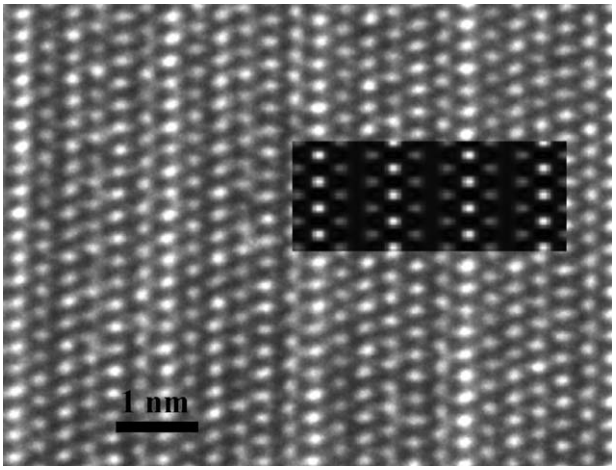

Fig. 2. HREM image of H-Ta_2O_5 in $92Ta_2O_5$–$8TiO_2$ along [$\bar{1}$ 1 0] zone axis. The inset is the simulated image.

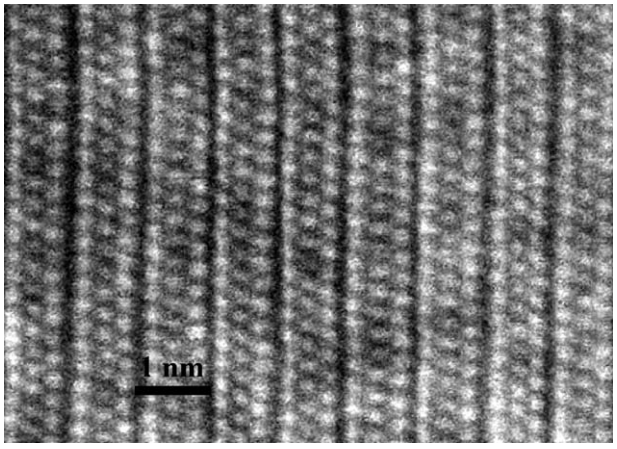

Fig. 3. HAADF image of H-Ta_2O_5 in $92Ta_2O_5$–$8TiO_2$ along [$\bar{1}$ 1 0] zone axis.

To explain both the electron diffraction data and HREM electron images, we propose a new structural model for H-Ta_2O_5. Fig. 4 illustrates the proposed structure. The new structure is comprised of hexagonal bi-pyramids and octahedral building blocks following the original idea of Stephenson and Roth, but now arranged in a different manner. Recall that in the previous model, the H-Ta_2O_5 structure consisted of idealized hexagonal bi-pyramids and distorted octahedra, with edge and corner sharing of oxygen anions. The pentagonal bi-pyramids in the experimentally determined structure can be considered as modifications of the idealized hexagonal bi-pyramids. Previously, there were 6 formula units per unit cell (12 tantalum atoms). The pentagonal bi-pyramids and octahedra were configured in a …-4-2-4-2-… sequence, with 4 octahedra followed by 2 hexagonal bi-pyramids. In our new model (Fig. 4), the pseudo-tetragonal structure is based on a …-2-1-2-1-… repetition of two octahedra followed by one hexagonal bi-pyramid. The basic molecular-building block is one hexagonal bi-pyramid edge shared with two octahedra, with 4 repetitions per unit cell. Fig. 4(a) illustrates the molecular configuration of the unit cell. The molecular-building blocks (Fig. 4(b)) are at cell positions (0, 0, 0), (0, 1/2, 1/4), (1/2, 1/2, 1/2) and (1/2, 0, 3/4), (Fig. 4(c)), and the cell is *body centered* with the extinction condition of structure factors $F_{hkl} \neq 0$, only if $h+k+l=2n$. The arrangement further results in a new extinction condition of structure factors $F_{hkl}=0$, if

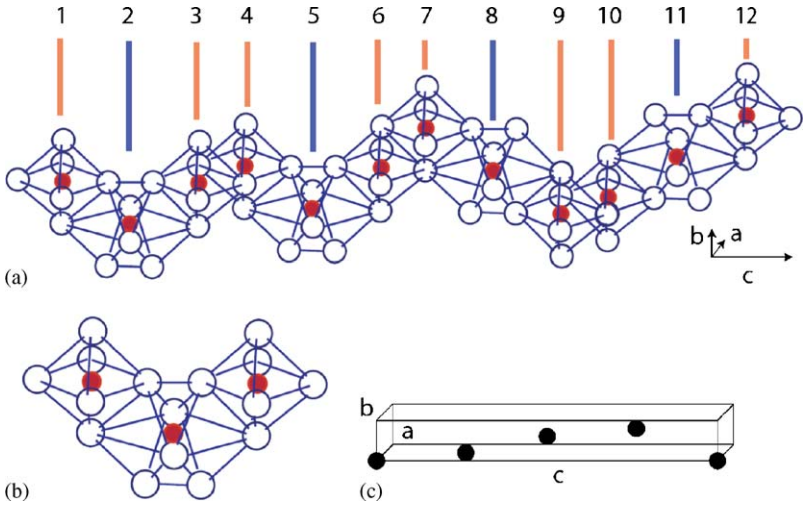

Fig. 4. The proposed structural model for H-Ta_2O_5 (a), consisting of molecular building blocks of edge-shared oxygen octahedra–hexagonal bi-pyramids–oxygen octahedra units with tantalum ions in their centers (b). The molecular building blocks repeat four times within the unit cell. The repeating pattern is shown in (c). The vertical lines denote the Ta positions in the …-2-1-2-1… sequence of …-2 octahedra-1 hexagonal bi-pyramid…-repeat units (a). The Ta atoms are labeled from 1 to 12.

$k + l/2 = 2n + 1$, in addition to the body-centered condition. The body-center extinction rule is consistent with the absence of (1, 0, 0), (−1, 1, $2l+1$) and (0, 0, $2n+1$) reflections in some zone axes. The new extinction condition does not allow (1, 1, 0) and (1, −1, 0) reflections along [001], and (1, 1, $4n$) and (0, 0, $4n+2$) along [110], which is consistent with electron diffraction data (Fig. 1). The (0, 0, 2) reflection along [100] can be attributed to double diffraction of the strong (0, 1, $2n+1$) reflections.

Our new model (Fig. 4) for the H-Ta_2O_5 structure consists of Ta coordinated in an octahedron–hexagonal bi-pyramid–octahedron molecular-building-block linkage. The model contains 12 Ta and 28 O per unit cell, which is 2 oxygen anions deficient for electro-neutrality in pure Ta_2O_5. The reduction in oxygen content comes from the change from a mixture of edge *and* corner sharing of oxygen octahedra–hexagonal bi-pyramids in the previous model to edge sharing *only* in the new model. Note, the change from corner to edge sharing can be achieved by crystallographic shear as suggested by Stephenson and Roth. However, shear alone does not account for the difference in the arrangement of oxygen octahedra and hexagonal bi-pyramids in these two models. The loss of oxygen in the model structure is assisted by TiO_2 substitution. For $x = 0.08$, the number of oxygen anions per unit cell reduces to 28.56 which is close to the 28 in our idealized structural model (Fig. 4(a)). For idealized edge sharing $x = 0.11$ would be required. For 29 oxygen anions per unit cell $x = 0.056$. At lower x values, there is a less deficiency of oxygen, and accommodation could be achieved by corner sharing of oxygen octahedra, which is observed in both the L-Ta_2O_5 structure and the H-Ta_2O_5 structure reported by Stephenson and Roth [12].

3.1.2. *Lattice imaging*

To check our model, we have simulated the HREM image for our proposed structure, and made comparisons with experimental data. Simulation was carried out by the Bloch-wave method [19] using the lens parameters of the high-resolution pole piece of the JEOL2010F and at different sample thickness and defocus. The best match with the experimental image was obtained at the thickness of 6–8 nm and a defocus of −80 nm. The result is shown in Fig. 2. The HREM simulation matches with the basic features of the experimental pattern, but not in some details. The main difference is the experimental HREM image has bright columns of dots separated by a distance of five columns, while the simulation has an extra column of bright dots in the middle separated by two columns.

To summarize Section 3.1, the H-Ta_2O_5 stabilized by $x = 0.08$ of TiO_2 differs from previously reported structural models. The basic structure for H-Ta_2O_5 is based on an pseudo-tetragonal unit cell (Fig. 4), but electron diffraction (Fig. 1) shows a monoclinic distortion. The role of TiO_2 substitutions on ionic displacements, modulated structures, and dielectric properties is now considered.

3.2. *Modulations of the H-Ta_2O_5 structure with TiO_2*

3.2.1. *Electron diffraction*

Experimentally, we observed systematic weak reflections (or super-structural reflections) in H-Ta_2O_5 as a function of TiO_2 substitution from $x = 0.03$ to 0.10. The weak reflections can be indexed by introducing a modulation vector $\mathbf{q}$: $\mathbf{g}_M = \mathbf{g}_m + \mathbf{q}$, where, M represents modulation and m monoclinic cell. Superstructure reflections observed for [$\bar{1}$ 1 0] and [001] zone axes give modulation vector $\mathbf{q}$

along $\langle 110 \rangle_{\text{tetragonal}}$ directions. The electron diffraction patterns along [100] and [010] zone axes show only the basic-structural reflections associated with the monoclinic cell. The modulation was also observed in the power spectrum of the HREM images recorded along [$\bar{1}$ 1 0]. The length of the primary modulation vector $|\mathbf{q}|$ were found to increase and then decrease with TiO_2 content. The intensity of the modulation reflection increased with increasing TiO_2 content.

Fig. 5 illustrates the electron diffraction pattern taken along the [001] zone axis for $97Ta_2O_5$–$3TiO_2$. Here, the modulation is along both the $\langle 110 \rangle_{\text{tetragonal}}$ directions. Along [110], the strongest super-structural reflection is at position $\mathbf{q} = (0.553, 0.553, 0) = (21/38, 21/38, 0)$, while that at $1 - \mathbf{q} = (0.447, 0.447, 0) = (17/38, 17/38, 0)$ is much weaker. Along the [$\bar{1}$ 1 0] direction, a strong super-structural reflection is visible at position $(-0.105, 0.105, 0) = (-4/38, 4/38, 0)$.

The superstructure is also visible along [$\bar{1}$ 1 0] and [$\bar{1}$ $\bar{1}$ 0] zone axes (Fig. 6). The electron diffraction patterns for the basic structure are equal for both zone axes. The super-structural reflections are situated at the same positions as observed previously along the [001] zone axis, however the intensity of reflections along the [110] direction is different. Here, the reflection at position (0.447, 0.447, 0) is much stronger than that at position (0.553, 0.553, 0) (see Figs. 6(a) and (b)).

The super-structural reflections along the [110] direction can be described by two incommensurate modulation vectors. The primary modulation vector $\mathbf{q}_1' = 0.553a^* + 0.553b^*$ produces a strong super-structural reflection at position (0.553, 0.553, 0) along the [001] zone axis, whereas the secondary modulation vector $\mathbf{q}_1'' = 0.447a^* + 0.447b^*$ produces a strong super-structural reflection at position (0.447, 0.447, 0) along the [$\bar{1}$ 1 0] zone axis. Along the [$\bar{1}$ 1 0] direction, the modulation is described by vector $\mathbf{q}_2 = -0.105a^* + 0.105b^*$.

The modulation vectors were found to change with increasing TiO_2 content. Fig. 7 gives the electron diffraction pattern along the [001] zone axis for $94.4Ta_2O_5$–$5.6TiO_2$. Here, the strong super-structural spot along the [110] direction is at position $\mathbf{q} = (0.550, 0.550, 0) = (11/20, 11/20, 0)$, while the super-structural spot at position $1 - \mathbf{q} = (0.450, 0.450, 0) = (9/20, 9/20, 0)$ is more weak. A much weaker spot at $(0.15, 0.15, 0) = (3/20, 3/20, 0)$, also seen in the electron diffraction pattern for the [001] zone axis, can be attributed to multiple electron scattering. Also in this specimen, the super-structural reflection at position $1 - \mathbf{q} = (9/20, 9/20, 0)$ appears strongest in some other zones (for example along [$\bar{1}$ 1 0]), which suggests that the $\mathbf{q}$ and $1-\mathbf{q}$ modulations co-exist in the crystal. Along the [$\bar{1}$ 1 0] direction, the super-structural reflections are at positions (−1/5, 1/5, 0). Thus, the modulation can be described by modulation vectors $\mathbf{q}_1' = 0.550a^* + 0.550b^*$, $\mathbf{q}_1'' = 0.450a^* + 0.450b^*$, and $\mathbf{q}_2 = -0.200a^* + 0.200b^*$.

For $94.4Ta_2O_5$–$5.6TiO_2$, a second modulated structure was sometimes observed in different fields of view. This modulation (not shown) gave similar electron diffraction patterns to Figs. 5 and 6, but with different modulation vectors for the occasional structure $\mathbf{q}_1' = 0.567a^* + 0.567b^*$ or (17/30, 17/30, 0), $\mathbf{q}_1'' = 0.433a^* + 0.433b^*$ or (13/30, 13/30, 0), and $\mathbf{q}_2 = -0.133a^* + 0.133b^*$ or (−4/30, 4/30, 0).

For increasing concentration of x, e.g., $92Ta_2O_5$–$8TiO_2$, the basic structure was modulated only in one of the $\langle 110 \rangle_{\text{tetragonal}}$ directions. Electron diffraction patterns along [$\bar{1}$ $\bar{1}$ 0] and [$\bar{1}$ 1 0] are given in Figs. 1(c) and (d). Along [$\bar{1}$ $\bar{1}$ 0], only the basic reflections are visible (Fig. 1(c)), but along [$\bar{1}$ 1 0] super-structural modulations are evident, with two nearly equal super-structural reflections at positions $(0.417, 0.417, 0) = (5/12, 5/12, 0)$ and $(0.583, 0.583, 0) = (7/12, 7/12, 0)$. A much weaker reflection at position (0.167, 0.167, 0) ≈ (2/12, 2/12, 0) is apparent (Fig. 1(d)). Super-structural reflections along the [110] direction are also visible in the electron diffraction

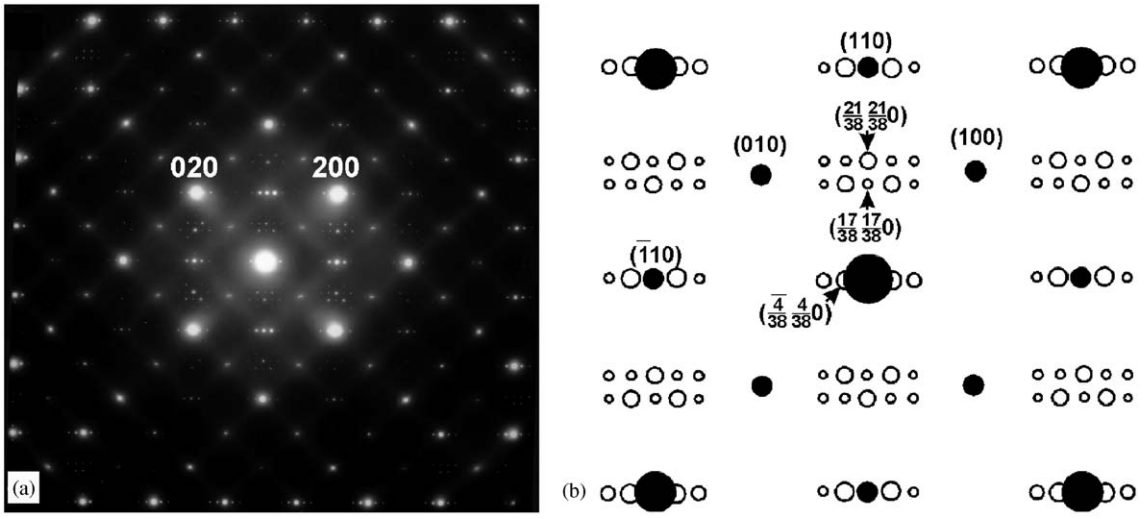

Fig. 5. Electron diffraction pattern for $97Ta_2O_5$–$3TiO_2$ along the [001] zone axis (a), and corresponding reciprocal plane (b).

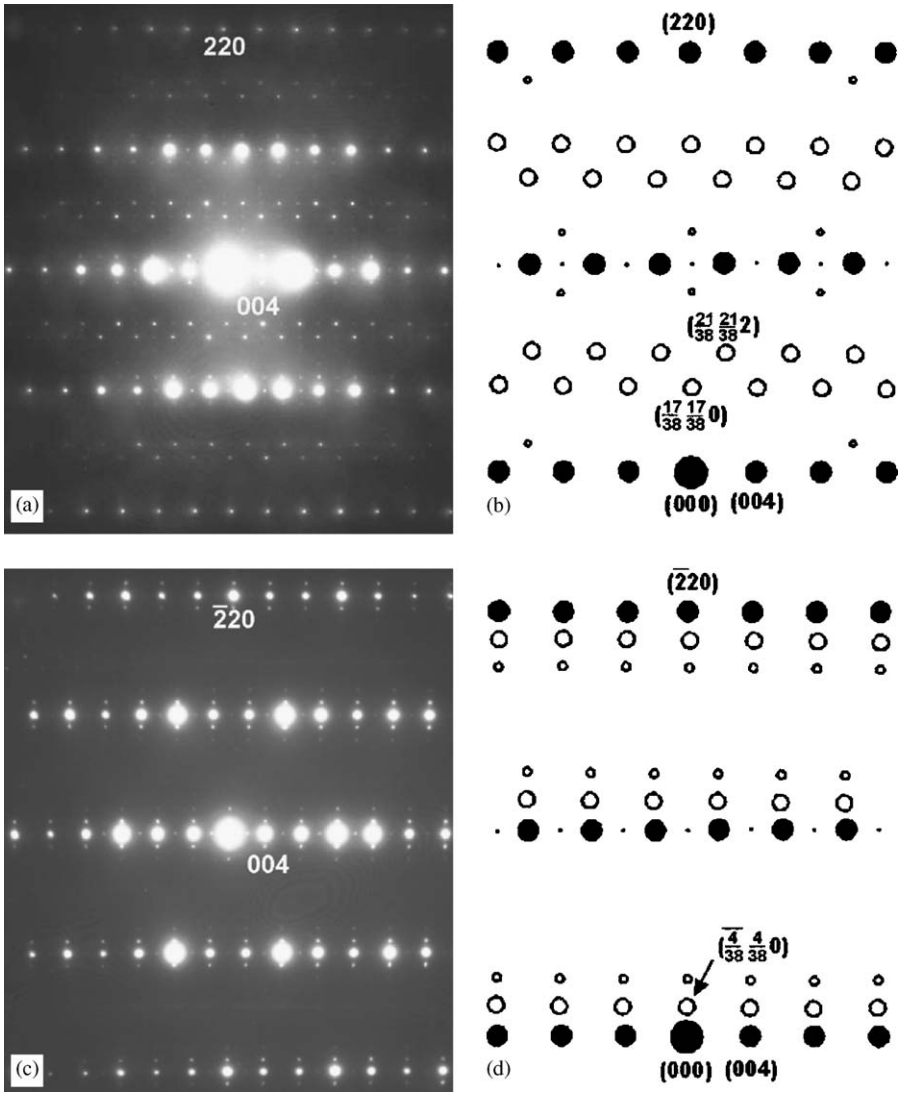

Fig. 6. Electron diffraction patterns for $97Ta_2O_5$–$3TiO_2$ along the [$\bar{1}$ 1 0] zone axis (a) and corresponding reciprocal plane (b); and, along the [$\bar{1}$ $\bar{1}$ 0] zone axis (c) and corresponding reciprocal plane (d).

pattern for the [001] zone axis (Fig. 1(c)). Equally intensive super-structural reflections can be interpreted in either one of two ways. The first is that there are two modulation vectors along [110]: $\mathbf{q}_1' = 0.583a^* + 0.583b^*$, and $\mathbf{q}_1'' = 0.417a^* + 0.417b^*$. The second possibility is that there is multiple scattering from one of the two modulation vectors. The first interpretation is in accordance with our HREM result (see discussion below). In addition, reflections at (0, 0, $2n$) and ($2n+1$, $2m+1$, 0) (n, m integer) positions are visible in the diffraction pattern along [$\bar{1}$ 1 0] ((Fig. 1(d)), which contains super-structural reflections, while they are not visible along [$\bar{1}$ $\bar{1}$ 0] (Fig. 1(c)).

The majority of electron diffraction patterns obtained for $92Ta_2O_5$–$8TiO_2$ were consistent with the superstructure described above, but, occasionally, another superstructure was observed. For this case, the modulation was along one of the $\langle 110 \rangle_{\text{tetragonal}}$ directions at position (0.154, 0.154, 0), and two equally strong reflections at positions (0.423, 0.423, 0) and (0.577, 0.577, 0).

For $90Ta_2O_5$–$10TiO_2$, the major diffraction patterns were consistent with the superstructure, with super-structural reflections at positions $(0.182, 0.182, 0) = (4/22, 4/22, 0)$, $(0.409, 0.409, 0) = (9/22, 9/22, 0)$, $(0.591, 0.591, 0) = (13/22, 13/22, 0)$, and at $(0.227, 0.227, 0) = (5/22, 5/22, 0)$ (Fig. 8).

In summary, the electron diffraction patterns obtained for H-Ta_2O_5 clearly show monoclinic distortions and modulations in the basic structure. Table 1 lists the possible vectors with increasing TiO_2 content. At low additions, e.g., 3 and 5.6 mol% TiO_2, the basic structure was modulated in both [110] and [$\bar{1}$ 1 0] directions. Along [110], the modulation vector $\mathbf{q}_1'$ and its complement $\mathbf{q}_1'' = 1 - \mathbf{q}_1'$ produced two super-structural reflections, which showed different intensities in the [001] and in [$\bar{1}$ 1 0] zone axes (see Figs. 5 and 6). In addition, the structure was modulated along [$\bar{1}$ 1 0] by $\mathbf{q}_2$ (see Figs. 5 and 6). For higher substitutions of TiO_2, e.g., 8 and 10 mol%, the basic structure was modulated only in one direction, along [110].

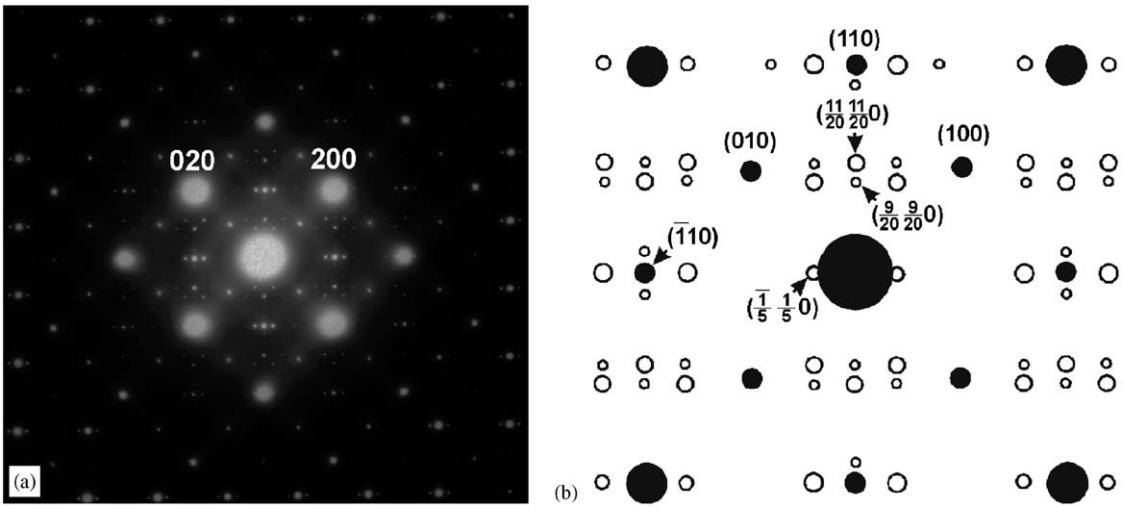

Fig. 7. Electron diffraction pattern for $94.4Ta_2O_5$–$5.6TiO_2$ along the [001] zone axis (a) and corresponding reciprocal plane (b).

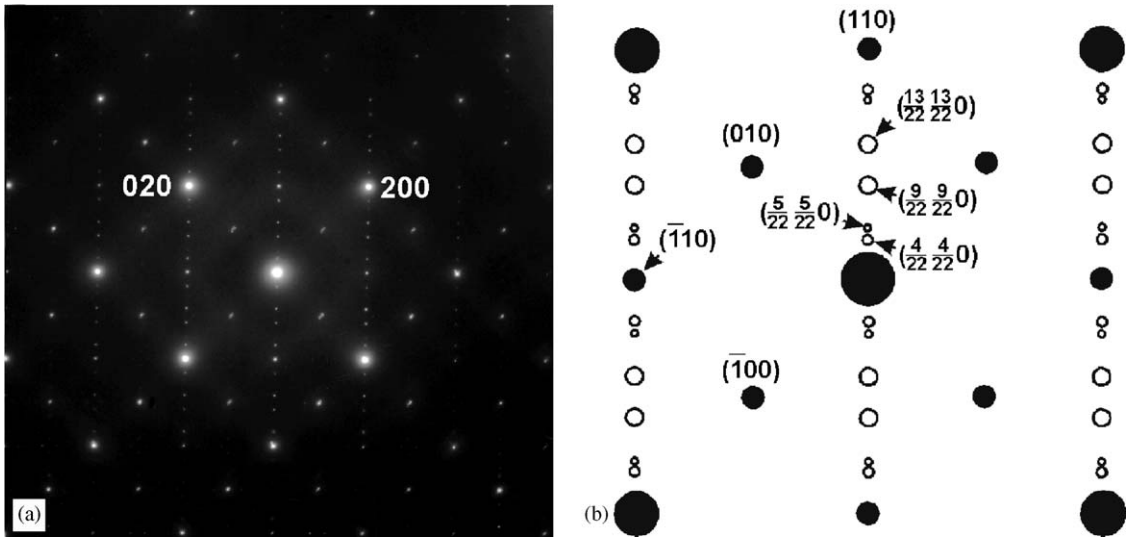

Fig. 8. Electron diffraction pattern for $90Ta_2O_5$–$10TiO_2$ along the [001] zone axis (a) and corresponding reciprocal plane (b).

Table 1
Modulation vectors

TiO_2 (mol%)	Modulation vector along [110] direction	Modulation vector along [$\bar{1}$ 1 0] direction
3	$\mathbf{q}_1' = 0.553a^* + 0.553b^*$ $\mathbf{q}_1'' = 0.447a^* + 0.447b^*$	$\mathbf{q}_2 = -0.105a^* + 0.105b^*$
5.6	$\mathbf{q}_1' = 0.550a^* + 0.550b^*$ $\mathbf{q}_1'' = 0.450a^* + 0.450b^*$ $\mathbf{q}_1' = 0.567a^* + 0.567b^*$ $\mathbf{q}_1'' = 0.433a^* + 0.433b^*$	$\mathbf{q}_2 = -0.133a^* + 0.133b^*$ $\mathbf{q}_2 = -0.200a^* + 0.200b^*$
8	$\mathbf{q}_1' = 0.583a^* + 0.583b^*$ $\mathbf{q}_1'' = 0.417a^* + 0.417b^*$ $\mathbf{q}_1' = 0.423a^* + 0.423b^*$ $\mathbf{q}_1'' = 0.577a^* + 0.577b^*$	No modulation No modulation
10	$\mathbf{q}_1' = 0.409a^* + 0.409b^*$ $\mathbf{q}_1'' = 0.591a^* + 0.591b^*$	No modulation

Here, the modulation produced two nearly intensive superstructural reflections (see Figs. 1(c) and (d)). These two reflections could be produced by two modulation vectors $\mathbf{q}_1'$ and $\mathbf{q}_1''$, or they could arise from double diffraction of one modulation vector ($\mathbf{q}_1'$ or $\mathbf{q}_1''$). Note, the primary modulation vector $\mathbf{q}_1'$ in Table 1, increases with increasing TiO_2 content, reaches a maximum value at $x = 0.08$, and decreases thereafter. (A secondary phase is known to exsolve above $x = 0.125$ [3].) A similar compositional dependence for the dielectric constant of the HT-phase is known, with a maximum K value around $x = 0.056$ or 0.08 [16–18]. The modulations are associated with Ti substitution and the related ionic displacements, and displacement or rotations of localized charge through a distance gives rise to dipoles and polarization phenomena. The results are in accordance with the enhancement of K for Ta_2O_5–TiO_2 ceramics.

3.2.2. High-resolution imaging

Electron diffraction results above identified a composition-dependent modulation of the monoclinic structure for H-Ta_2O_5 that maximized around $x = 0.08$. In Section 3.1, an idealized structural model was proposed based on edge-shared octahedral–hexagonal bi-pyramid–octahedra building blocks that repeat 4 times within a single prototypic tetragonal unit cell that was body centered. Now we present HREM images, in support of the modulation for $92Ta_2O_5$–$8TiO_2$, along one of the $\langle 110 \rangle$ directions.

Fig. 9(a) gives a HREM image for $92Ta_2O_5$–$8TiO_2$ taken along [$\bar{1}$ 1 0]. The corresponding electron diffraction pattern (Fig. 9(b)) identified superstructure spots at positions (0.423, 0.423, 0) (marked in Fig. 9(a) with $\mathbf{q}_1'$) and (0.577, 0.577, 0) ($\mathbf{q}_1''$). The HREM image was taken from an area away from the specimen edge where the super-structural reflections were clearly seen in the Fourier transform of the as-recorded HREM image (Fig. 9(c)). The image shows the same superstructure reflections as in the experimental electron diffraction pattern (Fig. 9(b)), which is a strong indication

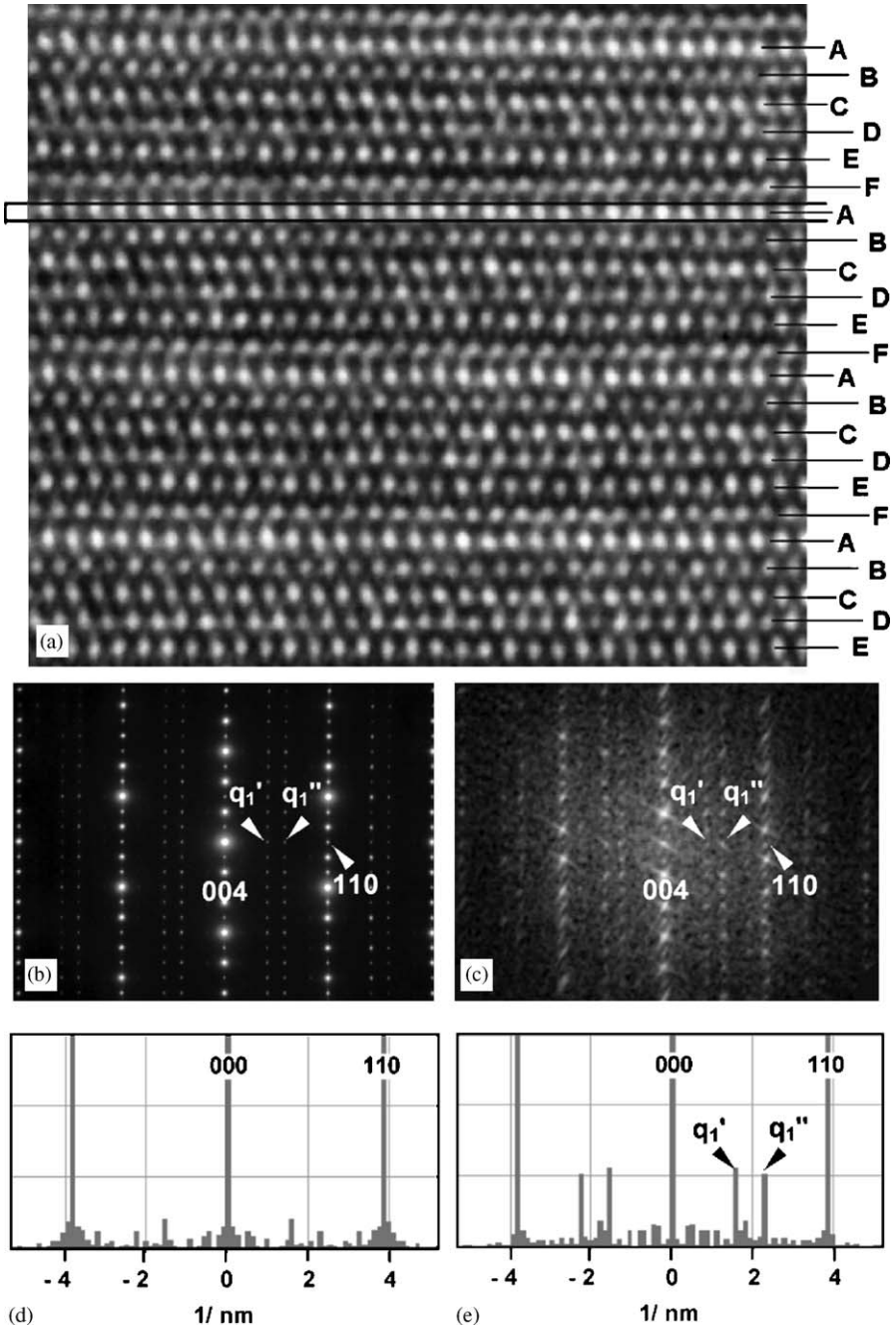

Fig. 9. HREM image of $92Ta_2O_5$–$8TiO_2$ along [$\bar{1}$ 1 0] zone axis (a), corresponding electron diffraction pattern (b), Fourier transform of the HREM image (c) and Fourier-transform graphs of the individual rows of bright spots along [110] direction, which are marked in the HREM image with "**A**" (d) and "**D**" (e). The modulation peaks (marked with $\mathbf{q}_1'$ and $\mathbf{q}_1''$) are visible in the FFT of rows marked with "**D**", while all the other rows of bright spots show only peaks due to the periodicity of the basic structure (d).

that the imaging condition was sensitive to detect the modulations. However, the amount of modulation was difficult to resolve by direct inspection of images.

Analysis of the HREM image revealed that the modulations were associated with distortions in certain (0, 0, l) planes from the pseudo-tetragonal structure. The HREM image for the [$\bar{1}$ 1 0] zone axis can be described as a repeat of six rows of bright spots (**A**, **B**, **C**, **D**, **E**, **F**; see Fig. 9(a)) associated with the (0, 0, 12) planes. The Fourier-transform function (FFT) for each row was used to detect modulations along the [110] direction in each row. An example of the area of the HREM image used in the 1-D FFT calculation is indicated in Fig. 9(a) for row "**A**". The FFT graph of the individual row of bright spots associated with the (0, 0, 12) plane shows two strong peaks that correspond to the (110) periodicity (Fig. 9(d)). In rows marked by "**D**", two additional periodicities were detected (Fig. 9(e)). The positions for these two peaks identified in **D** rows (marked by $\mathbf{q}_1'$ and $\mathbf{q}_1''$ in Fig. 9(e)) match perfectly with the positions of the super-structural spots in the experimental diffraction pattern (0.423, 0.423, 0) and (0.577, 0.577, 0) in Fig. 9(b).

The results suggest that the modulations occur periodically in one of the (0, 0, 12) planes. From our previous discussion of the idealized structure, we now propose a modification for the actual H-Ta_2O_5 structure. In this model, the rows of bright spots are associated with the hexagonal bi-pyramids (the position of hexagonal bi-pyramids is indicated in Fig. 4). Compared with the experimental image, the simulated HREM image (see inset in Fig. 2) has two extra rows of bright spots at the position of the fifth row, **D**. Our analysis of HREM images suggests a modification of hexagonal bi-pyramids at the position of the fifth and 11th rows (see Fig. 4), which we attribute to Ti incorporation, that will compensate for the oxygen deficiency in Ta_2O_5 doped with 8 mol% TiO_2.

The modulation of the basic structure is associated with a monoclinic distortion. The measured monoclinic angle for Ta_2O_5 doped with 8 mol% TiO_2 is $\beta \approx 90.8^\circ$. The monoclinic distortion of the pseudo-tetragonal structure is in *a*–*b* plane, with the 2-fold axis along the *c*-axis. The lack of a mirror perpendicular to the *c*-axis in our model would eliminate monoclinic point group 2/*m*, leaving one of the two remaining monoclinic point groups, 2 or *m*, which are polar. Thus, the monoclinic distortion leads to an acentric structure. Acentricity has been confirmed by second-harmonic signal generation. If the spontaneous polarization directions in polycrystalline H-Ta_2O_5 could be poled with an applied field, they would become piezoelectric and ferroelectric ceramics. Their susceptibility to induced polarization with a weak field is reflected in the enhanced values of dielectric constant ($K = 100-300$) reported for Ta_2O_5–TiO_2 ceramics with the H-Ta_2O_5 structure.

4. Conclusions

The structure of high-temperature solid solutions in the series $(1-x)Ta_2O_5$–$xTiO_2$ were investigated at room temperature by TEM, electron diffraction and high-resolution imaging. Based on the evidence of electron diffraction and imaging, we derived a new structural model for H-Ta_2O_5 based on an edge-sharing of oxygen octahedron–hexagonal bi-pyramid–octahedron unit that repeat four times per unit cell. The structure is monoclinic. Modulations of the basic structure were also observed by electron diffraction; the modulation was primarily along $\langle 110 \rangle$. The modulation length varied with increasing TiO_2 substitution. Row-by-row Fourier analysis of HREM lattice images showed that the modulation was associated with Ti substitution of Ta and the related small ionic displacements in specific lattice planes. The results are of interest for an understanding of dielectric properties.

Acknowledgments

This material is based upon work supported by the US Department of Energy, Division of Materials Sciences under Award No. DEFG02-91ER45439, through the Frederick Seitz Materials Research Laboratory at the University of Illinois at Urbana-Champaign. Research for this publication was carried out in the Center for Microanalysis of Materials, University of Illinois at Urbana-Champaign, which is partially supported by the US Department of Energy under Award no. DEFG02-91-ER45439. The work was carried out while Dr. Darko Makovec was a Fulbright Scholar at the University of Illinois at Urbana-Champaign. The authors would also like to thank the Fulbright Commission for financing his stay. Collaborations with Geoff Brennecka and Sarunya Hemjinda are gratefully acknowledged.

References

[1] A. Reisman, F. Holtzberg, M. Barkenblit, M. Berry, J. Am. Chem. Soc. 78 (1956) 4514.
[2] S.P. Gerg, N. Krishnamurthy, A. Awasthi, M. Venkatraman, J. Phase Equilibria 17 (1996) 63.
[3] J.L. Waring, R.S. Roth, J. Res. Nat. Bur. Stan. 72A (1968) 175.
[4] R.S. Roth, J.L. Waring, J. Res. Nat. Bur. Stan. 74A (1970) 485.
[5] N.C. Stephenson, R.S. Roth, Acta Crystallogr. B 27 (1971) 1037.
[6] B.O. Marinder, J. Solid State Chem. 160 (2001) 62.
[7] C. Askeljung, B.O. Marinder, M. Sundberg, J. Solid State Chem. 176 (2003) 250.
[8] L.A. Aleshina, S.V. Loginova, Cryst. Rep. 47 (2002) 415.
[9] N. Terao, Jpn. J. Appl. Phys. 6 (1967) 21.
[10] A. Fukumoto, K. Miwa, Phys. Rev. B 55 (1997) 11155.
[11] M. Hiratami, S. Kimura, T. Hamada, S. Iijima, N. Nakanishi, Appl. Phys. Lett. 81 (2002) 2433.
[12] R.S. Roth, J.L. Waring, J. Res. Nat. Bur. Stan. 74A (1970) 477.
[13] W. Mertin, R. Gruehn, H. Schaefer, J. Solid. State Chem. 1 (1970) 425.
[14] N.C. Stephenson, R.S. Roth, J. Solid State Chem. 3 (1971) 145.
[15] V. Von Plies, R. Gruehn, Z. Anorg. Allg. Chem. 463 (1980) 32.
[16] R.F. Cava, W.F. Peck Jr., J.J. Krajewski, Nature 377 (1995) 215.
[17] S. Henjimda, Thesis, University of Illinois at Urbana, Champaign, Urbana, IL, 2001.
[18] G.L. Brennecka, D.A. Payne, J. Am. Ceram. Soc., in press.
[19] J.M. Zuo, J. Mabon, Microscopy and Microanalysis 10 (2004) 1000.